Penerbit Akademia Baru

CFD Letters

Journal homepage: www.akademiabaru.com/cfdl.html
ISSN: 2180-1363

Flow and Heat Transfer Characteristic of Inclined Oval Trench Dimples With Numerical Simulation

Open Access

Ibroheng piya[1], Pathomporn Narato[1], Makatar Wae-hayee[1], Chayut Nuntadusit[1,*]

[1] Department of Mechanical Engineering, Faculty of Engineering, Prince of Songkla University, Hat Yai, Songkhla 90112, Thailand

ARTICLE INFO

Article history:
Received 23 September 2020
Received in revised form 22 November 2020
Accepted 24 November 2020
Available online 29 November 2020

ABSTRACT

In this work, flow and heat transfer in a channel having oval trench dimples were investigated numerically. 3-D channel flow with a cross-section of 300-mm width and 32-mm height were created using Computational Fluid Dynamic (CFD) with ANSYS, Fluent (V.15.0). Five oval trench dimples with 3-mm depth, 10.0-mm width and 45-mm length arranging with a single row and in-line configuration were located on the bottom surface of the channel. Reynolds number based on hydraulic diameter of the channel were fixed at Re=20,000 whereas a dimple inclined angle defined as the angle of dimple centreline to the mainstream was varied at 0, 15, 30 and 45 degrees. $k-\omega$ SST turbulent model was used to solve governing Equations. The result show that longitudinal vortex flow occurred at θ=15° to 45° which would be enhance heat transfer on the surface. When inclined angle became larger, the areas of Nusselt number and high total pressure coefficient took place at dimple edge in +Z direction. The peak of average spanwise Nusselt numbers took place for the case of θ=45°. Moreover, the area of high spanwise average Nusselt numbers ($\overline{Nu}$>100) for the case θ=30° was the largest.

Keywords:
Oval-trench dimples; inclined angle; heat transfer enhancement; CFD

1. Introduction

Heat transfer enhancement on a surface using turbulent generators is popularly applied in thermal industrial equipment. Heat transfer enhancement mechanism is that flow passing these turbulator disturbs both thermal and velocity boundary layers by generating several complex flows such as separation, attachment, circulation, longitudinal vortex, etc. Another heat transfer enhancement mechanism by installing these turbulators are to enlarge heat transfer area. Typical these turbulators are ribs, pins, blockages, triangular wing, hemispherical protrusion, or dimple. Most popular turbulator which ware widely applied and comprehensively studied is dimple due to less pressure drop penalty as compared to other turbulators, affecting on increasing thermal performance. Several applications of applying dimple in thermal equipment are cooling part of automotive, compact heat exchangers, micro-channel [1-4], etc.

* *Corresponding author.*
E-mail address: chayut@me.psu.ac.th (Chayut Nuntadusit)

https://doi.org/10.37934/cfdl.12.11.6171

Flow structure passing dimple cavity is comprehensively studied. Moon *et al.,* [5] have reported similar flow pattern passing over dimple when a channel height is in the range of 0.37<H/d <1.49 [5]. Typical flow structures passing over the dimples is presented in Figure 1. Flow separates in half upstream dimple forming recirculation flow. At this region, extremely low heat transfer occurs. Then, flow attaches on half downstream dimple resulting on high heat transfer in this area. Moreover, upwash flow, which is formed from attachment flow, mixes with bulk flow generating longitudinal vortex pair over smooth surface along downstream of dimple. More details of flow patterns are reported in the previous studies [6-8].

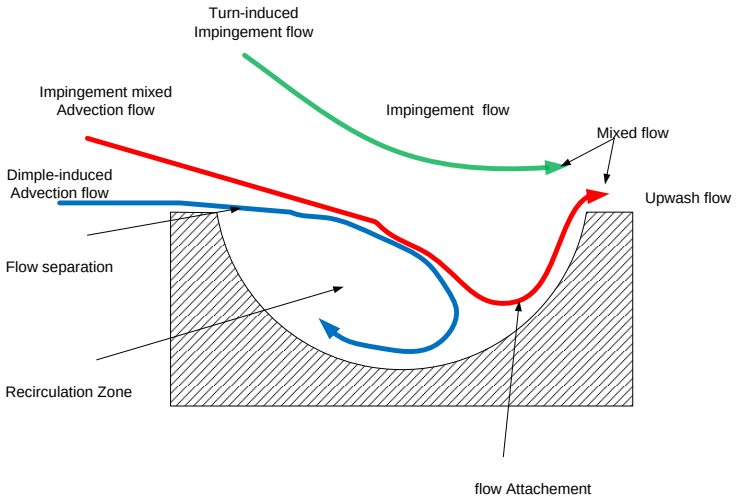

Fig. 1. The flow Structure passing over a circular dimple

As aforementioned above, classical dimple geometry is circular or hemispherical dimple. Deferent dimple geometries affect directly on flow structure and heat transfer characteristics. Xie *et al.,* [9] investigated symmetrical and asymmetrical dimple cavity, numerically. It was found that flow through the symmetrical dimple generated circulation flow within upstream dimple cavity, resulting heat transfer in this area. When designing asymmetric dimple cavity, the circulation flow disappeared casing high local heat transfer in this region.

Rao *et al.,* [10] studied the effect of circular shape and ellipsoid shape of dimple. The results showed that ellipsoid shape has slightly lower heat transfer and slightly higher friction factors as compared to the case of circular shape. The heat transfer distributions on dimple different geometries as square, triangular, circular, and teardrop were studied by the previous scholars [11,12]. The results showed that the teardrop dimple has the highest heat transfer. More details of investigation on dimple geometry are reported in the previous studies [13-17].

Recently, Isaev *et al.,* [18] studied oval-trench dimple which was inclined to main stream. However, they are focused at fixed inclined angle at 45°. Hence, the main idea proposed in this work is to vary inclined angle of oval-trench dimple with single row under fully developed flow. result in it would show the best angle that most heat transferable. So, it can be used to increase efficiency and steady temperature in lithium-ion batteries.

2. Methodology

2.1 Computational Model and Boundary Conditions

A Numerical model of rectangular wind tunnel forming with oval-trench dimples is shown in Figure 2. A cross-section of the tunnel was 300-mm width and 32-mm height, and a length of the tunnel was 1900 mm for the first section, 350 mm for test section and 950 mm for the last section.

An origin of the Cartesian coordinates was assigned on the bottom wall of the wind tunnel in the test section area. The Y-axis and the Z-axis were on the orthogonal plane normal to the mainstream, and the X-axis was along the axial of the mainstream. A uniform velocity with the magnitude of 5.49 m/s, corresponding to Re=20,000, was assigned at the velocity inlet. A row of five oval-trench dimples was formed on the bottom surface of the tunnel. The centreline of dimple row was assigned at X/D=0.

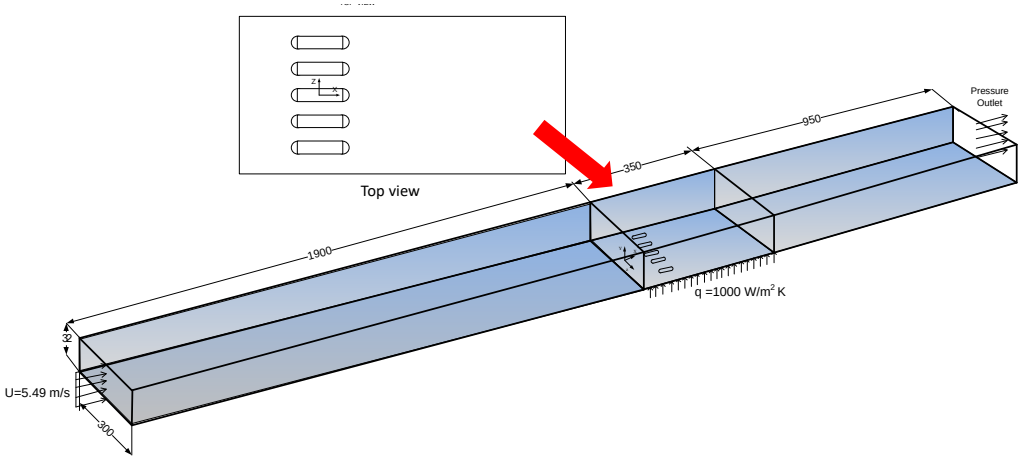

Fig. 2. A simulation model of wind tunnel with oval-trench dimples

Figure 3 shows the schematic outline of an oval-trench dimple. A length and a wide of the dimple were 55 mm and 10 mm, respectively. A depth and a depth radial of the dimple were 3 mm and r=5.67 mm. These dimensions were referenced from similar dimple configuration as oval shape [19].

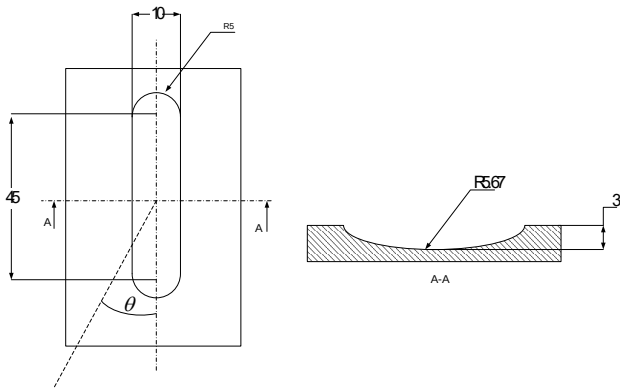

Fig. 3. Configuration of oval-trench dimple

For boundary condition, the uniform velocity at 5.49 m/s was set at velocity inlet, and pressure at 0 Pa was set at pressure outlet. The heated surface where the dimples were formed was assigned as constant heat flux. The details of boundary conditions are shown in Table.1.

Table 1
The details of boundary conditions

Boundary condition	Define
Constant velocity inlet	5.49 m/s
Front and far side surface	wall
Top and bottom surfaces	wall
Pressure outlet	0 Pa
Constant heat flux	1000 W/K.m^2

2.2 Governing Equation

The governing Equation of the fluid flow and heat transfer which include the conservation of the mass, momentum and energy are [20]

The mass conservation

$$\frac{\partial(\rho u_i)}{\partial x_i} = 0 \tag{1}$$

The momentum conservation

$$\frac{\partial(\rho u_i u_j)}{\partial x_j} = -\frac{\partial P}{\partial x_i} + \frac{\partial}{\partial x_j}\left(\mu\left(\frac{\partial u_j}{\partial x_i} + \frac{\partial u_i}{\partial x_j}\right)\right) \tag{2}$$

The energy conservation

$$\frac{\partial(\rho u_i T)}{\partial x_i} = \frac{\partial}{\partial x_i}\left(\frac{\lambda}{c_p}\frac{\partial T}{\partial x_j}\right) \tag{3}$$

The turbulent kinetic energy equation k and the dissipation rate ω equation

$$\frac{\partial}{\partial x_i}(\rho k u_j) = \tilde{P}_k - \beta^* \rho \omega k + \frac{\partial}{\partial x_j}\left[(\mu + \sigma_k \mu_t)\frac{\partial k}{\partial x_j}\right] \tag{4}$$

$$\frac{\partial(\rho\omega)}{\partial x_j} = \alpha\rho S^2 - \beta\rho\omega^2 + \frac{\partial}{\partial x_j}\left[(\mu + \sigma_\omega \mu_t)\frac{\partial \omega}{\partial x_j}\right] + 2\rho(1-F_1)\sigma_{\omega 2}\frac{1}{\omega}\frac{\partial k}{\partial x_j}\frac{\partial \omega}{\partial x_j} \tag{5}$$

The production term $\tilde{P}_k = \tau_{ij}(\partial u_i / \partial x_j)$ and the Reynolds stress τ_{ij} are related to the mean strain-rate tensor S_{ij} through the Boussinesq approximation

$$\tau_{ij} = 2\mu_t\left(S_{ij} - \frac{1}{3}S_{kk}\delta_{ij}\right) - \frac{2}{3}\rho k\delta_{ij}, \qquad S_{ij} = \frac{1}{2}\left(\frac{\partial u_i}{\partial x_j} + \frac{\partial u_j}{\partial x_i}\right)$$

The kinematic eddy viscosity is given by

$$\upsilon_t = \frac{\alpha_1 k}{\max(\alpha_1 \omega, SF_2)}$$

where $a_1 = 0.31$ and $S = \sqrt{2S_{ij}S_{ij}}$ is the absolute value of the mean strain-rate tensor. Other model parameters are

$$P_\omega = \gamma \frac{p_k}{\upsilon_t}, \qquad F_1 = \tanh\left(\xi^4\right),$$

$$\xi = \min\left[\max\left\{\frac{\sqrt{k}}{\beta^* \omega y}, \frac{500\upsilon}{\omega y^2}\right\}, \frac{4\sigma_{\omega 2} k}{CD_\omega y^2}\right]$$

$$CD_\omega = \max\left(\frac{2\sigma_{\omega 2}}{\omega}\frac{\partial k}{\partial x_i}\frac{\partial \omega}{\partial x_i}, 10^{-10}\,\mathrm{s}^{-2}\right)$$

$$F_2 = \tanh\left[\left\{\max\left(\frac{2\sqrt{k}}{\beta^* \omega y}, \frac{500\upsilon}{\omega y^2}\right)\right\}^2\right]$$

where v is the kinematic viscosity. The model coefficients in Eqs. (1) and (2) are obtained from

$$\left(\sigma_k \sigma_\omega \beta\right)^T = F_1\left(\sigma_k \sigma_\omega \beta\right)_1^T + \left(1 - F_1\right)\left(\sigma_k \sigma_\omega \beta\right)_2^T$$

With the following values

$$\sigma_{k1} = 0.85, \quad \sigma_{\omega 1} = 0.5, \quad \beta_1 = 0.075 \quad \sigma_{k2} = 1.0, \quad \sigma_{\omega 2} = 0.856, \quad \beta_{21} = 0.0827,$$

the coefficient γ is

$$\gamma = \frac{\beta}{\beta^*} - \frac{\kappa^2}{\sigma_\omega \sqrt{\beta^*}}$$

with $\kappa = 0.41$ and $\beta^* = 0.09$.

2.3 Grid Generation and Grid Dependency

In numerical simulation study, mesh quality must be evaluated to achieve accurate results from the effect of mesh number. Figure 4 shows grid generation in test section area where a row of dimples was formed. The number of the generated grid was varied in the range of 4 to 8.3 million elements. The effect of variation of grid number on Nusselt number distributions along the centerline of dimple row is shown in Figure 5. These results show that Nusselt Numbers do not change significantly when the mesh number increases from 5.0 million to 7.0, 8.3 million. Therefore, a mesh number of 5.0 million for the computation domain was adopted in this study for all parameters.

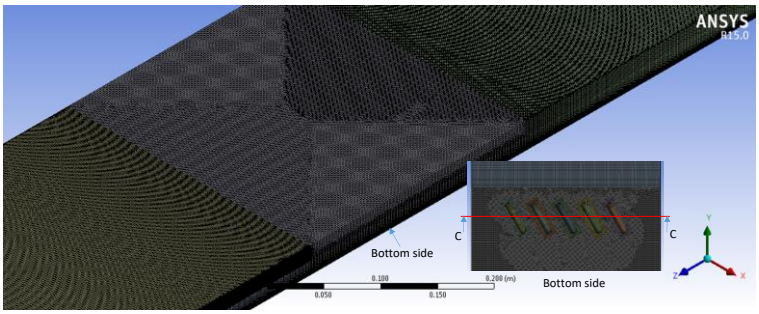

Fig. 4. Grid generation at test section area

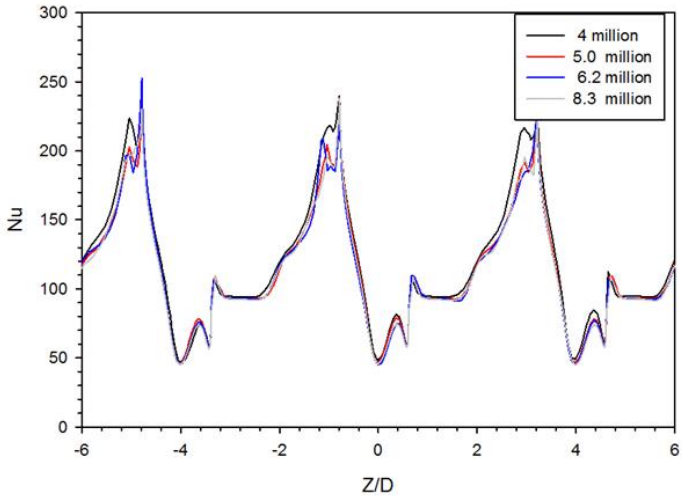

Fig. 5. The effect of variation of grid number on Nusselt number distributions along the centerline of dimple row

2.4 Calculation Method and Algorithm

Computations were conducted by solving Reynolds averaged continuity, Navier-Stokes, and energy equations under steady state conditions. In this work, $k-\omega\ SST$ turbulence model was used because it can provide similar predicted reattachment flow on the surface and it can generate strong longitudinal vortex flow results of Oval-trench dimples problems. Moreover, this model can accurately predict the solutions of heat transfer problems with moderate computation cost. The SIMPLE algorithm was used with second order upwind scheme for all spatial discretization. The convergence of iterative solution was insured when the residual of all the variables was less than the specified value was 1×10^{-4}.

2.5 Parameter Definitions

The parameters employed in this study are described follow. The Reynolds number, Re, is given by

$$Re = \frac{VD}{v} \tag{6}$$

where V are the mean velocity of the channel at origin of test section, v are the kinematic viscosity of air at 303 K. Distribution of the total pressure coefficient which is defined as

$$C_p = \frac{(p-p_o)}{0.5\rho V^2} \tag{7}$$

where p , p_o are the static pressure at the point of the oval-trench dimple surface and the static pressure before the oval-trench dimple; ρ, V are the density and mean velocity of the channel at origin of test section. The local heat transfer coefficient (h) can then be evaluated from Eq. (4)

$$h = \frac{\dot{q}}{(T_w-T_m)} \tag{8}$$

where q are the heat losses from wall to surrounding, T_w is the local wall temperature, T_m is the average temperature from origin of test section to dimple downstream.
The local Nusselt number (Nu) is calculated using Eq. (5)

$$Nu = \frac{\mathrm{hD}}{\mathrm{k}} \tag{9}$$

where D are the hydraulic diameter of the rectangular channel and k are thermal conductivity of air.

3. Results

3.1 Flow Characteristics

Figure 6 shows streamlines over oval-trench dimples. At θ=0° (Figure 6(a)), it can be seen that small recirculation flow appears at the upstream of oval-trench dimple. Then, the streamlines flow parallelly along longitudinal axis of the dimple. At θ=15° (Figure 6(a)), small recirculation flow appears at the upstream of the dimple, similarly as previously shown for the case of θ=0°. At this case, small longitudinal vortex flow was generated along downstream of the dimple. This longitudinal vortex flow became larger when inclined angle was larger as θ=30° and 45° (Figure 6(c) and (d)).

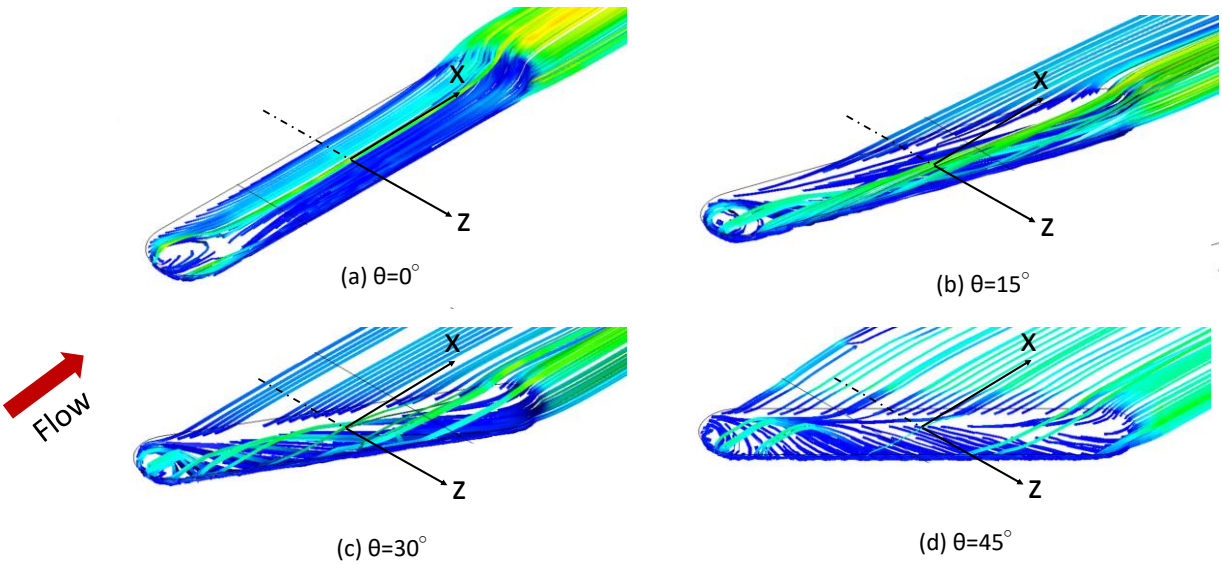

Fig. 6. 3-D streamline distributions on dimple with different inclined angles at Re=20,000 (Dash line is the centerline of dimple row)

3.2 Total Pressure Coefficients Characteristics

Figure 7. shows the total pressure coefficient distributions on a heated surface of the bottom of the wind tunnel in area of -6<Z/D<6 and -4<X/D<8. It shows that high total pressure coefficient took place in upstream region while low total pressure coefficient appeared in downstream region. At θ=0° (Figure 7(a)), the total pressure coefficient is symmetry in Z-axis.

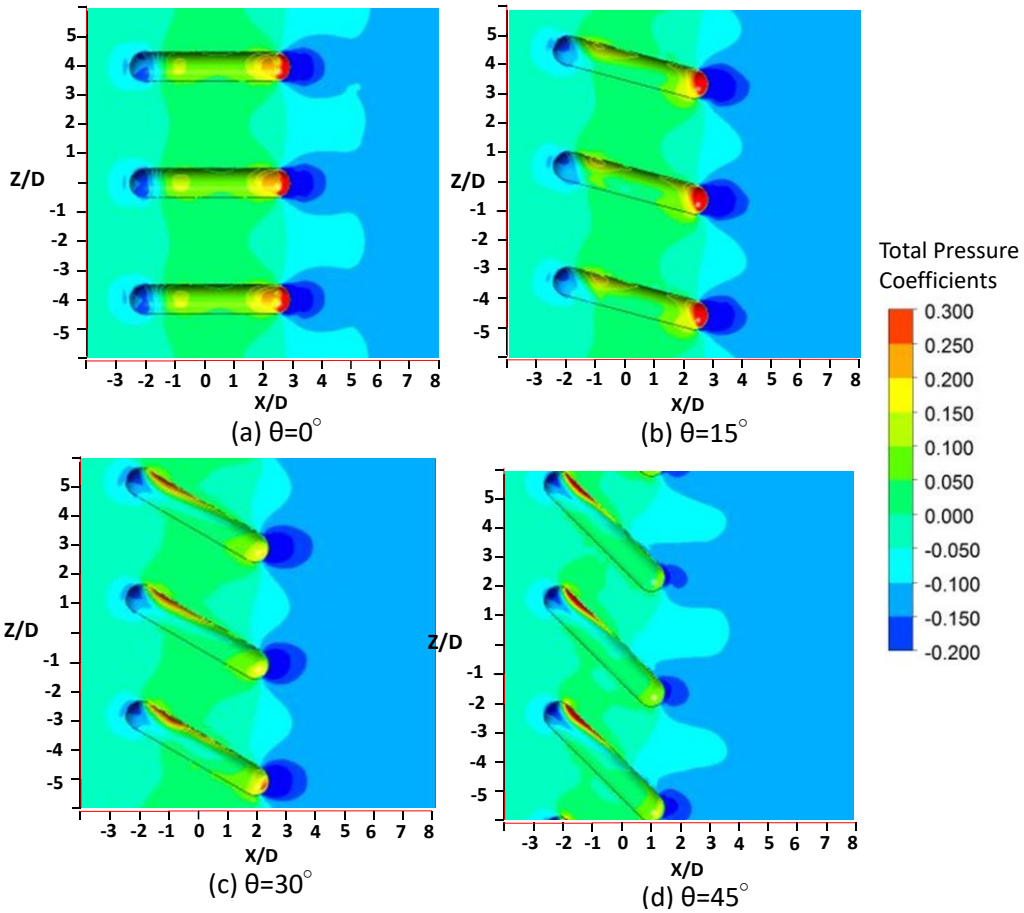

Fig. 7. Total pressure coefficient fields on a heated surface of the bottom of the wind tunnel (Re=20,000)

When inclined angle become θ=15° (Figure 7(b)), area of high total pressure coefficient is also inclined in +Z direction. This high area of total pressure coefficient at the upstream of every dimple in +Z direction can be clearly seen when the angles became larger at θ=30° (Figure 7(c)) and θ=45° (Figure 7(d)). This area of total pressure coefficient distributions would be effect on heat transfer enhancement which would be discussed in the next section.

3.3 Local Nusselt Numbers Characteristics

Local Nusselt number distributions on a heated surface of the bottom of the wind tunnel in area of -6<Z/D<6 and -4<X/D<8 are shown in Figure 8. Generally, Nusselt number distributions were high in upstream region and low in downstream region. This corresponded to the characteristics of total pressure coefficient distributions as previously shown in Figure 7.

At θ=15° (Figure 8(b)), the Nusselt number distribution is quite different when compared to the case of At θ=0° (Figure 8(a)). The area at dimple edge in +Z direction of θ=15° were higher than that of θ=0°. This high Nusselt number is from the effect of inclined angle generating longitudinal vortex flow as previously shown in Figure 6. Longitudinal vortex flow became larger when inclined angle was larger. This also affected on larger area of Nusselt number when inclined angle was larger as θ=30° and θ=45° (Figure 8(c) and (d)).

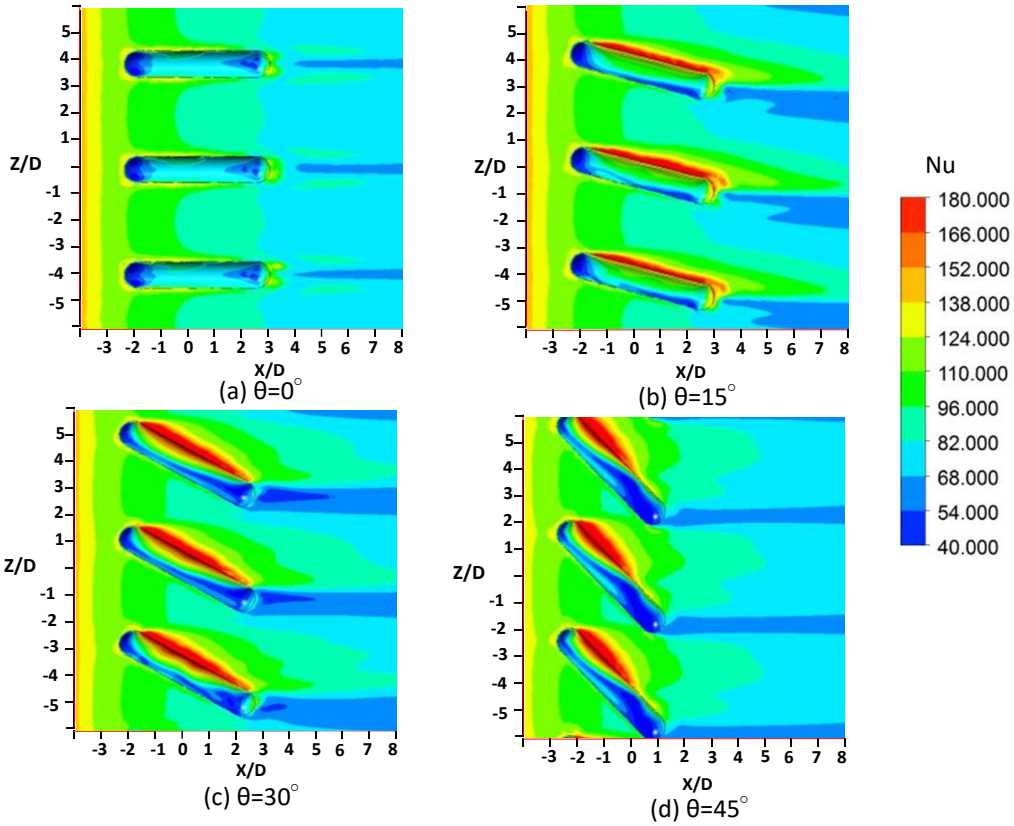

Fig. 8. Local Nusselt number distributions on a heated surface of the bottom of the wind tunnel (Re=20,000)

3.4 Spanwise Average Nusselt Numbers

Spanwise average Nusselt numbers which were calculated in the range of -6<Z/D<6 is shown in Figure 9. Noted that this average number included area of dimple cavity. Generally, spanwise average Nusselt numbers of θ=0° is lower than the other cases, exception in the rage of 2.5<Z/D<3.5, which is higher than the case of θ=30° and θ=45°. When the inclined angle become larger, the peak of spanwise average Nusselt numbers is higher. In addition, it was found that an area of high spanwise average Nusselt numbers ($\overline{Nu}$>100) for the case θ=30° was larger than the other cases.

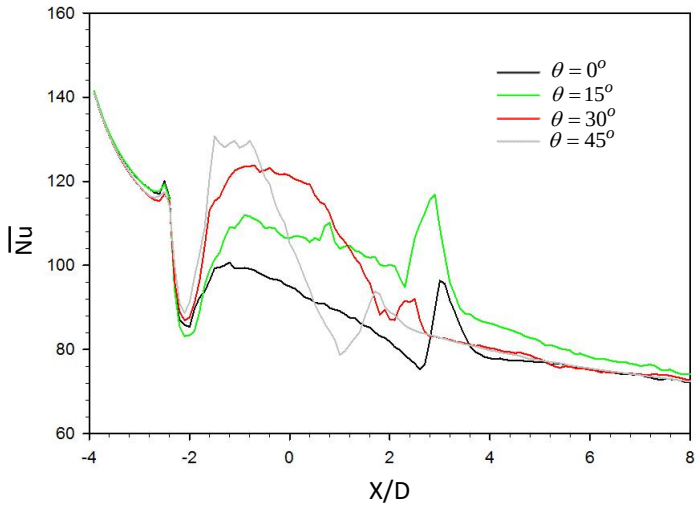

Fig. 9. Spanwise Average Nusselt numbers in the range of -6<Z/D<6 (Re=20,000)

4. Conclusions

Effects of oval trench dimple angle on heat transfer enhancement and flow characteristics have been numerically investigated in this study. Main results can be summarized as follows

i. At θ=15° to 45°, longitudinal vortex flow occurred. This cased to enhance heat transfer on the surface.
ii. Area of high Nusselt number corresponded to the area of high total pressure coefficient. When inclined angle became larger, the areas of Nusselt number and high total pressure coefficient took place at dimple edge in +Z direction.
iii. The peak of average spanwise Nusselt numbers took place for the case of θ=45°.
iv. The area of high spanwise average Nusselt numbers ($\overline{Nu}$ >100) for the case θ=30° was larger than the other cases.

Acknowledgement

This research was funded by a grant from the Department of Mechanical Engineering, Faculty of Engineering, Prince of Songkla University, Thailand and by Energy Technology Research Center.

References

[1] Wang, Yiping, Shuai Li, Xu Xie, Yadong Deng, Xun Liu, and Chuqi Su. "Performance evaluation of an automotive thermoelectric generator with inserted fins or dimpled-surface hot heat exchanger." *Applied Energy* 218 (2018): 391-401. https://doi.org/10.1016/j.apenergy.2018.02.176
[2] Lu, Gaofeng, and Xiaoqiang Zhai. "Analysis on heat transfer and pressure drop of a microchannel heat sink with dimples and vortex generators." *International Journal of Thermal Sciences* 145 (2019): 105986. https://doi.org/10.1016/j.ijthermalsci.2019.105986
[3] Soman, Divya P., S. Karthika, P. Kalaichelvi, and T. K. Radhakrishnan. "Experimental study of turbulent forced convection heat transfer and friction factor in dimpled plate heat exchanger." *Applied Thermal Engineering* 162 (2019): 114254. https://doi.org/10.1016/j.applthermaleng.2019.114254
[4] Nascimento, Idário P., and Ezio C. Garcia. "Heat transfer performance enhancement in compact heat exchangers by using shallow square dimples in flat tubes." *Applied Thermal Engineering* 96 (2016): 659-670. https://doi.org/10.1016/j.applthermaleng.2015.11.042
[5] Moon, H. K., T. O'connell, and B. Glezer. "Channel height effect on heat transfer and friction in a dimpled passage." *J. Eng. Gas Turbines Power* 122, no. 2 (2000): 307-313. https://doi.org/10.1115/1.483208
[6] Xie, Gongnan, and Bengt Sundén. "Numerical predictions of augmented heat transfer of an internal blade tip-wall by hemispherical dimples." *International journal of heat and mass transfer* 53, no. 25-26 (2010): 5639-5650. https://doi.org/10.1016/j.ijheatmasstransfer.2010.08.019
[7] Kovalenko, G. V., V. I. Terekhov, and A. A. Khalatov. "Flow regimes in a single dimple on the channel surface." *Journal of applied mechanics and technical physics* 51, no. 6 (2010): 839-848. https://doi.org/10.1007/s10808-010-0105-z
[8] Tay, C. M., Y. T. Chew, B. C. Khoo, and J. B. Zhao. "Development of flow structures over dimples." *Experimental Thermal and Fluid Science* 52 (2014): 278-287. https://doi.org/10.1016/j.expthermflusci.2013.10.001
[9] Xie, Yonghui, Huancheng Qu, and Di Zhang. "Numerical investigation of flow and heat transfer in rectangular channel with teardrop dimple/protrusion." *International Journal of Heat and Mass Transfer* 84 (2015): 486-496. https://doi.org/10.1016/j.ijheatmasstransfer.2015.01.055
[10] Rao, Yu, Bo Li, and Yan Feng. "Heat transfer of turbulent flow over surfaces with spherical dimples and teardrop dimples." *Experimental Thermal and Fluid Science* 61 (2015): 201-209.

https://doi.org/10.1016/j.expthermflusci.2014.10.030
[11] Rao, Yu, Yan Feng, Bo Li, and Bernhard Weigand. "Experimental and numerical study of heat transfer and flow friction in channels with dimples of different shapes." *Journal of Heat Transfer* 137, no. 3 (2015). https://doi.org/10.1115/1.4029036
[12] Acharya, Sumanta, and Fuguo Zhou. "Experimental and computational study of heat/mass transfer and flow structure for four dimple shapes in a square internal passage." *Journal of Turbomachinery* 134, no. 6 (2012). https://doi.org/10.1115/1.4006315
[13] Liu, Jing, and Jie Li. "Numerical Prediction of Flow Structure and Heat Enhancement with Different Dimple Depth." In *Applied Mechanics and Materials*, vol. 574, pp. 147-153. Trans Tech Publications Ltd, 2014. https://doi.org/10.4028/www.scientific.net/AMM.574.147
[14] Katkhaw, Nopparat, Nat Vorayos, Tanongkiat Kiatsiriroat, Yottana Khunatorn, Damorn Bunturat, and Atipoang Nuntaphan. "Heat transfer behavior of flat plate having 45 ellipsoidal dimpled surfaces." *Case Studies in Thermal Engineering* 2 (2014): 67-74. https://doi.org/10.1016/j.csite.2013.12.002
[15] Turnow, Johann, Nikolai Kornev, Valery Zhdanov, and Egon Hassel. "Flow structures and heat transfer on dimples in a staggered arrangement." *International Journal of Heat and Fluid Flow* 35 (2012): 168-175. https://doi.org/10.1016/j.ijheatfluidflow.2012.01.002
[16] Sethi, Muneesh, and N. S. Thakur. "Correlations for solar air heater duct with dimpled shape roughness elements on absorber plate." *Solar Energy* 86, no. 9 (2012): 2852-2861. https://doi.org/10.1016/j.solener.2012.06.024
[17] Oo, Ye Min, Makatar Wae-hayee, Kamil Abdullah, and Chayut Nuntadusit. "The effect of hemispherical dimple spacing on flow structure and heat transfer characteristics of internal flow using CFD." *Songklanakarin Journal of Science & Technology* 41, no. 5 (2019).
[18] Isaev, S. A., A. I. Leontiev, O. O. Milman, I. A. Popov, and A. G. Sudakov. "Influence of the depth of single-row oval-trench dimples inclined to laminar air flow on heat transfer enhancement in a narrow micro-channel." *International Journal of Heat and Mass Transfer* 134 (2019): 338-358. https://doi.org/10.1016/j.ijheatmasstransfer.2018.12.175
[19] Isaev, Sergey, Mikhail Gritckevich, Alexandr Leontiev, and Igor Popov. "Abnormal enhancement of separated turbulent air flow and heat transfer in inclined single-row oval-trench dimples at the narrow channel wall." *Acta Astronautica* 163 (2019): 202-207. https://doi.org/10.1016/j.actaastro.2019.01.033
[20] Rahman, M. M., V. Vuorinen, J. Taghinia, and M. Larmi. "Wall-distance-free formulation for SST k-ω model." *European Journal of Mechanics-B/Fluids* 75 (2019): 71-82. https://doi.org/10.1016/j.euromechflu.2018.11.010